0026-895X/95/030611-13$3.00/0

MOLECULAR PHARMACOLOGY, 47:611–623, 1995.

Polymorphism-Structure Relationships of Rifamexil, an Antibiotic Rifamycin Derivative

ALESSIA BACCHI, GIOVANNI MORI, GIANCARLO PELIZZI, GIORGIO PELOSI, MARINO NEBULONI, and GIAN BATTISTA PANZONE

Dipartimento di Chimica Generale ed Inorganica, Chimica Analitica, Chimica Fisica, and Centro di Studio per la Strutturistica Diffrattometrica del C.N.R., I-43100 Parma, Italy (A.B., G.M., G.Peli., G.Pelo.), and Lepetit Research Center, Gerenzano (Varese), I-21040 Italy (M.N., G.B.P.)

Received September 19, 1994; Accepted December 9, 1994

SUMMARY

The polymorphism of rifamexil, a rifamycin derivative, has been investigated by thermomicroscopy, differential thermal analysis (differential scanning calorimetry-thermogravimetry), IR spectroscopy, and X-ray powder diffraction. Two crystalline forms, an amorphous material, and three solvates have been studied. The crystal structures of two solvates have also been determined by single-crystal X-ray techniques. Although the overall conformation of rifamexil is very similar in the two compounds, marked differences occur between the two crystal packings, due to differences both in the mutual orientation of the molecules and in the rifamexil-solvent interactions. Multivariate statistical methods have been used to identify the principal structural parameters determining the biological activity of the rifamycins.

The polymorphism of drugs is a matter of great importance, especially because different polymorphs may have different properties (such as dissolution rate and physical and chemical stability) that can be related to biological activity (1–4). In past decades efforts have been made not only to detect and characterize the various forms of drugs but also to obtain information on the structural parameters responsible for the polymorphism. With this aim a study was undertaken of the solid state of rifamexil [2′-(diethylamino)rifamycin P], an antibiotic rifamycin derivative obtained from a semi-synthesis of natural rifamicyn S produced from *Streptomyces mediterranei* (5). Rifamexil is active against *Mycobacterium avium complex* and other slowly and rapidly growing mycobacteria that are the causative agents of infections in patients with acquired immunodeficiency syndrome.

Several studies on the relationship of structural features to the activity of a series of rifamycin derivatives have appeared, and in many cases relationships between conformation and biological activity have been investigated; some authors have proposed models for a possible interaction with the enzyme DNA-dependent RNA polymerase, on the basis of X-ray crystal structure elucidation (6–11). Rifamycins are very likely to be polymorphic, because their complex structures display a number of different possibilities for hydrogen bonding, conformation, and ionization and consequently allow different crystalline packings to occur. Until now polymorphism of rifampicin (12), rifandin (13, 14), and rifamycin S (15, 16) has been reported, but a single-crystal X-ray analysis has been carried out for only two polymorphic forms of rifamycin S.

In this paper five modifications of rifamexil, i.e., two crystalline forms, one amorphous form, and three solvates with organic solvents, are described and characterized by thermomicroscopy, DSC-TG, IR spectroscopy, and X-ray powder diffraction. Moreover, a single-crystal X-ray diffraction analysis has been carried out on two solvates, showing the crystalline cohesion to be due to hydrogen bonds between rifamexil and the solvent molecules.

Materials and Methods

Pure rifamexil sample, prepared following the synthesis reported in Ref. 5, was used as starting material for polymorphic form preparation. Form I was obtained by thermal modification of form II at 190°, whereas form II was obtained by thermal treatment of the ethanol solvate at 110°. The amorphous form was obtained by grinding of form I or form II or by rapid evaporation of a chloroform solution; solvate SI (with 0.5 mol of ethyl acetate) was obtained by the heating at 60° of a crystalline powder isolated from ethyl acetate solution at 40°. Solvate SII (with 1 mol of ethyl acetate and 0.5 mol of water) was obtained by slow crystallization of rifamexil from ethyl acetate solution at room temperature. Solvate SIII (with 1 mol of ethanol and 1 mol of water) was obtained by slow crystallization from 95% ethanol solution at room temperature. All of the polymorphic forms are slightly hygroscopic and have never been obtained without water of imbibition.

The nature of the solvents crystallized in the solvates was identi-

ABBREVIATIONS: DSC, differential scanning calorimetry; TG, thermogravimetry; PCA, principal-component analysis; PC, principal component; DF, discriminant function; FT, Fourier-transformed.

fied by gas chromatography. Thermal analysis was carried out with a DuPont TA 2000 instrument equipped with a DSC cell and a TG module. The working conditions were as follows: gas flow, N_2 at 25 ml/min; heating rate, 10°/min; open sample aluminium pan; sample weight, 4 mg. Thermomicroscopy involved Kofler hot-stage microscopy with polarized light. The IR spectra were recorded with a FT-IR Bruker model IFS 48 spectrophotometer, in Nujol mull. X-ray powder diffraction spectra were obtained with Philips (PW 1010/77, 1049/01, or 4025/10) instruments, by using CuKα radiation.

Irregularly shaped, reddish-orange crystals suitable for X-ray diffraction work were obtained from ethyl acetate solution (SII) or ethanol solution (SIII). The crystal system and orientation matrix were obtained in each case by use of automatic peak search and indexing procedures. The crystal lattice of SII was determined to be monoclinic with systematic absences characteristic of space groups $P2_1/m$ and $P2_1$, with the latter being the only one possible in view of the optical activity of the compound, whereas SIII was found to be orthorhombic and to belong to the uniquely determined space group $P2_12_12_1$. Table 1 summarizes the relevant data concerning the two analyses. The lattice parameters were determined from angular settings of 30 reflections measured on an automatic Siemens AED single-crystal diffractometer equipped with an IBM PS2/30 personal computer; nickel-filtered CuKα radiation was used. Intensity data were collected on the same instrument by the $\theta/2\theta$ scan method, with a drive speed related to the number of counts in the peak. Although the crystal used for X-ray work was of good size in each case, the number of observed data points is rather low, due to a steady intensity decrease (more relevant in SIII) throughout data collection and to a rapid fall-off at high-angle reflection intensities (there were very few detectable reflections at values of $2\theta > 100°$). The reflections were processed with the peak profile procedure (17) and corrected for crystal decay and for Lorentz and polarization effects.

Both crystal structures are remarkable in that the asymmetric unit comprises two chemically identical but crystallographically independent rifamexil molecules. In each case the structure determination was not straightforward, i.e., a complete structure was not developed *ab initio* from the default run of phasing techniques, and the E maps, especially in the case of SII, revealed only planar sets of cross-linked hexagons. After many unsuccessful attempts, the two structures were finally solved by the direct-methods program SIR88 (18), which gave a nearly 30-atom fragment containing the aromatic moieties. Several successive cycles of structure factor and difference Fourier series calculations carried out by means of the SHELX76 package of crystallographic computer programs (19) made it possible to complete both structures, which were refined by full-matrix least-squares fitting to minimize the quantity $\Sigma w(|F_o| - |F_c|)^2$, with parameters grouped into two blocks. It is worth noting that these structures are undoubtedly among the largest ones without a heavy atom (127 or 124 nonhydrogen atoms/asymmetric unit) reported to date that have been solved by direct methods. For SII the *y*-value for the atom S1 (molecule A) was fixed to determine the origin along the *b*-axis. Because of the limited amount of observed data, not all of the atoms, i.e., only those belonging to the fused-ring system and the associated O1, O2, O4, N1, and N3 atoms, were refined anisotropically. The numbering system used is illustrated in Fig. 1. In each case the X-ray analysis revealed the presence of solvents of crystallization; associated with the two independent rifamexil molecules present in the asymmetric unit of each compound there are two molecules of ethyl acetate and one of water in SII and two molecules of ethanol and two of water in SIII. The hydrogen atoms were ignored in spite of the presence of some electron density in the expected regions. No peak of chemical significance was present in the final Fourier difference maps. For both compounds the enantiomorph chosen has the correct absolute configuration at C20, which was known to be *S*. This allows assignment of absolute configuration at the other eight asymmetric carbon atoms, i.e., C12(*S*), C21(*S*), C22(*R*), C23(*R*), C24(*R*), C25(*S*), C26(*R*), and C27(*S*). The weak diffracting power of the crystals and their instability to X-ray radiation are both responsible for the somewhat high values of the final residuals (SII, $r = 0.0884$, $R_w = 0.1187$; SIII, $r = 0.1030$, $R_w = 0.1283$. Fractional atomic coordinates are listed in Tables 2 and 3, together with equivalent isotropic thermal parameters. All calculations were performed on a GOULD SEL 6040 computer. In addition to the aforementioned programs, PARST (20), ORTEP (21), and PLUTO (22) have been used.

TABLE 1

Crystallographic data and data collection and refinement procedures for compounds SII and SIII

Parameter	SII	SIII
Formula	$C_{46}H_{64}N_3O_{13.5}S$	$C_{44}H_{63}N_3O_{13}S$
Molecular weight	907.08	874.05
Crystal system	Monoclinic	Orthorhombic
Space group	$P2_1$	$P2_12_12_1$
a (Å)	18.857 ± 8	31.319 ± 9
b (Å)	18.168 ± 8	27.669 ± 8
c (Å)	15.889 ± 6	11.624 ± 4
β°	108.53 ± 2	
V (Å^3)	5,161 ± 4	10,073 ± 5
Z	4	8
D_{calc} (g/cm^3)	1.167	1.153
μ (cm^{-1})	10.30	10.31
F(000)	1,940	3,744
Number of reflections measured	7,488	6,428
Number of unique reflections	7,156	6,392
Condition for observed reflections	$I > 2\sigma(I)$	$I > 3\sigma(I)$
Number of observed reflections	4,017	3,416
Parameters refined	729	731
Maximal height in final ΔF map (*e*/Å^3)	0.51	0.41
R	0.0884	0.1019
R_W	0.1187	0.1284

Results and Discussion

Polymorphic Forms. Rifamexil shows polymorphism, which is believed to be due to the various possibilities for hydrogen-bonding, for conformational exchanges, and for ionization states that allow different crystalline packings to occur. Rifamexil was initially described as a red crystalline substance melting at 160–180° (5), and so it appears to be

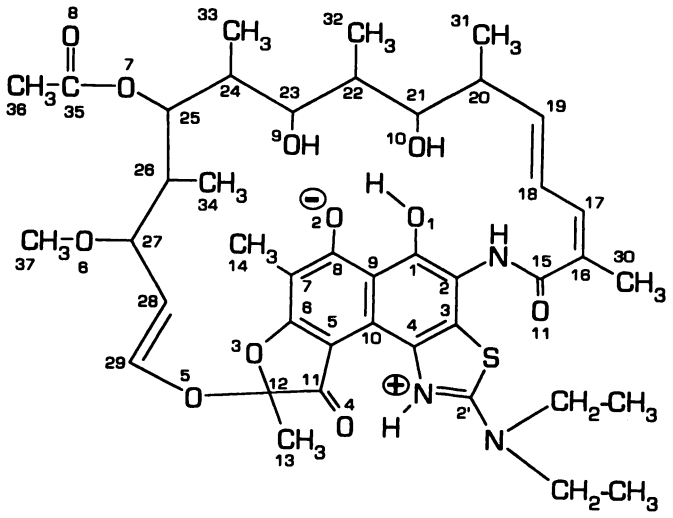

Fig. 1. Chemical diagram of rifamexil.

TABLE 2

Compound SII atomic coordinates (× 10^4) and equivalent isotropic thermal parameters (one third trace of the diagonalized matrix), with standard deviations

Atom	Molecule A				Molecule B			
	x/a	*y/b*	*z/c*	U_{eq} (× 10^4)	*x/a*	*y/b*	*z/c*	U_{eq} (× 10^4)
				Å²				Å²
S1	−634 ± 2	−4020 ± 0	−5771 ± 3	779 ± 18	2741 ± 2	88 ± 2	−2953 ± 2	608 ± 15
O1	−1571 ± 5	−1320 ± 5	−6167 ± 7	709 ± 44	4044 ± 5	1517 ± 5	−4898 ± 6	616 ± 40
O2	−2211 ± 6	−848 ± 5	−5191 ± 8	843 ± 52	4308 ± 6	2809 ± 5	−4594 ± 7	710 ± 44
O3	−2731 ± 6	−2379 ± 6	−3040 ± 7	833 ± 49	3529 ± 5	4058 ± 5	−2450 ± 6	647 ± 42
O4	−2026 ± 6	−4129 ± 6	−3432 ± 7	830 ± 51	2577 ± 6	2680 ± 5	−1653 ± 7	712 ± 46
O5	−1997 ± 6	−3141 ± 6	−1909 ± 7	780 ± 29	3674 ± 5	3893 ± 5	−958 ± 7	637 ± 25
O6	−22 ± 7	−1908 ± 7	−1580 ± 8	988 ± 36	5760 ± 5	2721 ± 5	−171 ± 6	691 ± 26
O7	1568 ± 5	−3045 ± 5	−1368 ± 7	730 ± 27	5415 ± 5	888 ± 6	409 ± 7	713 ± 27
O8	1935 ± 7	−1945 ± 7	−692 ± 8	1044 ± 37	6592 ± 8	1204 ± 7	1165 ± 9	1098 ± 42
O9	2067 ± 5	−1766 ± 6	−2776 ± 7	757 ± 28	6653 ± 5	437 ± 6	−1051 ± 7	723 ± 27
O10	1764 ± 5	−1765 ± 6	−4595 ± 7	765 ± 29	6078 ± 6	−308 ± 6	−2619 ± 7	797 ± 29
O11	−911 ± 6	−3420 ± 7	−7444 ± 7	885 ± 31	2602 ± 5	−499 ± 5	−4672 ± 6	721 ± 27
N1	−771 ± 6	−2350 ± 6	−6651 ± 7	649 ± 50	3630 ± 6	217 ± 6	−4476 ± 8	599 ± 47
N2	−1356 ± 6	−4081 ± 6	−4639 ± 8	655 ± 51	2715 ± 6	1360 ± 6	−2283 ± 7	531 ± 46
N3	−577 ± 7	−5105 ± 6	−4577 ± 10	849 ± 65	2328 ± 7	458 ± 6	−1518 ± 8	653 ± 51
C1	−1548 ± 8	−1994 ± 8	−5800 ± 11	641 ± 66	3694 ± 8	1500 ± 7	−4276 ± 9	562 ± 57
C2	−1190 ± 7	−2547 ± 8	−6090 ± 9	540 ± 55	3445 ± 7	839 ± 7	−4057 ± 9	514 ± 53
C2′	−875 ± 8	−4464 ± 8	−4936 ± 11	696 ± 69	2561 ± 8	666 ± 7	−2153 ± 10	555 ± 61
C3	−1151 ± 8	−3249 ± 7	−5650 ± 10	618 ± 60	3095 ± 7	836 ± 7	−3411 ± 9	539 ± 55
C4	−1497 ± 7	−3371 ± 8	−5031 ± 8	555 ± 58	3030 ± 7	1475 ± 7	−2971 ± 8	512 ± 56
C5	−2171 ± 8	−2879 ± 7	−4026 ± 10	600 ± 61	3240 ± 8	2826 ± 7	−2715 ± 8	553 ± 54
C6	−2464 ± 8	−2256 ± 9	−3750 ± 11	703 ± 69	3561 ± 7	3468 ± 7	−2961 ± 9	520 ± 54
C7	−2527 ± 8	−1576 ± 8	−4123 ± 9	610 ± 62	3931 ± 8	3493 ± 7	−3556 ± 10	623 ± 64
C8	−2241 ± 9	−1489 ± 8	−4800 ± 11	698 ± 68	3960 ± 8	2829 ± 8	−4029 ± 11	696 ± 68
C9	−1891 ± 7	−2107 ± 8	−5120 ± 10	608 ± 59	3628 ± 7	2171 ± 6	−3836 ± 9	474 ± 51
C10	−1861 ± 7	−2813 ± 7	−4741 ± 8	475 ± 51	3305 ± 7	2162 ± 7	−3149 ± 9	490 ± 53
C11	−2221 ± 8	−3459 ± 11	−3487 ± 10	701 ± 68	2926 ± 8	3023 ± 8	−2074 ± 9	584 ± 59
C12	−2530 ± 8	−3130 ± 10	−2742 ± 11	794 ± 76	3148 ± 7	3827 ± 7	−1839 ± 10	539 ± 57
C13	−3224 ± 9	−3552 ± 10	−2671 ± 11	805 ± 45	2509 ± 8	4349 ± 9	−1857 ± 10	738 ± 43
C14	−2873 ± 9	−906 ± 9	−3829 ± 11	870 ± 47	4270 ± 11	4203 ± 11	−3778 ± 13	959 ± 55
C15	−669 ± 8	−2767 ± 9	−7278 ± 10	717 ± 40	3195 ± 7	−397 ± 7	−4801 ± 8	506 ± 31
C16	−221 ± 9	−2461 ± 9	−7796 ± 11	804 ± 46	3522 ± 8	−902 ± 8	−5289 ± 9	576 ± 36
C17	538 ± 10	−2356 ± 10	−7444 ± 12	886 ± 50	4170 ± 8	−1265 ± 8	−4885 ± 9	567 ± 35
C18	974 ± 9	−2544 ± 9	−6474 ± 10	768 ± 43	4591 ± 8	−1220 ± 8	−3971 ± 10	666 ± 39
C19	1689 ± 11	−2509 ± 10	−6217 ± 12	920 ± 54	5242 ± 8	−1578 ± 8	−3607 ± 9	621 ± 36
C20	2201 ± 9	−2792 ± 10	−5303 ± 11	797 ± 46	5693 ± 7	−1581 ± 7	−2626 ± 9	563 ± 34
C21	1934 ± 9	−2558 ± 9	−4561 ± 10	734 ± 43	5707 ± 7	−818 ± 7	−2167 ± 9	577 ± 36
C22	2473 ± 9	−2750 ± 9	−3591 ± 10	761 ± 43	6088 ± 7	−791 ± 7	−1211 ± 9	564 ± 34
C23	2132 ± 8	−2541 ± 8	−2885 ± 10	659 ± 39	6139 ± 7	−28 ± 7	−776 ± 8	480 ± 30
C24	1371 ± 8	−2901 ± 8	−2975 ± 10	664 ± 39	5389 ± 7	408 ± 8	−1027 ± 9	583 ± 35
C25	1086 ± 7	−2691 ± 8	−2198 ± 9	572 ± 35	5552 ± 7	1096 ± 7	−417 ± 8	480 ± 31
C26	302 ± 9	−2927 ± 9	−2278 ± 11	755 ± 43	4983 ± 8	1722 ± 7	−791 ± 9	604 ± 37
C27	74 ± 10	−2680 ± 10	−1475 ± 11	821 ± 47	5088 ± 7	2366 ± 7	−179 ± 8	510 ± 33
C28	−722 ± 11	−3073 ± 11	−1585 ± 12	936 ± 54	4426 ± 8	2853 ± 9	−363 ± 10	691 ± 39
C29	−1360 ± 9	−2747 ± 9	−1913 ± 10	773 ± 43	4345 ± 9	3464 ± 9	−784 ± 11	760 ± 44
C30	−673 ± 13	−2232 ± 14	−8779 ± 16	1349 ± 78	3069 ± 9	−979 ± 9	−6249 ± 10	782 ± 44
C31	2329 ± 13	−3608 ± 13	−5312 ± 15	1199 ± 68	5336 ± 8	−2150 ± 9	−2149 ± 10	741 ± 41
C32	3215 ± 10	−2368 ± 10	−3438 ± 12	893 ± 51	6875 ± 9	−1149 ± 9	−926 ± 10	770 ± 43
C33	1427 ± 10	−3768 ± 10	−3066 ± 12	901 ± 50	4753 ± 8	−59 ± 8	−909 ± 10	701 ± 41
C34	−189 ± 15	−2676 ± 15	−3165 ± 18	1423 ± 86	5048 ± 9	1987 ± 9	−1727 ± 11	787 ± 43
C35	1974 ± 9	−2604 ± 10	−696 ± 11	788 ± 43	6012 ± 9	992 ± 9	1182 ± 10	742 ± 41
C36	2406 ± 11	−3032 ± 12	70 ± 14	1108 ± 62	5744 ± 11	776 ± 11	1958 ± 13	1075 ± 61
C37	−30 ± 13	−1568 ± 13	−782 ± 16	1274 ± 72	6131 ± 9	3108 ± 10	644 ± 11	818 ± 46
C38	72 ± 12	−5386 ± 12	−4776 ± 14	1104 ± 61	2218 ± 9	989 ± 9	−852 ± 10	746 ± 41
C39	−187 ± 14	−5965 ± 15	−5540 ± 17	1388 ± 82	2911 ± 10	1096 ± 11	−115 ± 12	983 ± 54
C40	−839 ± 9	−5477 ± 9	−3900 ± 11	798 ± 45	2078 ± 9	−314 ± 9	−1479 ± 11	791 ± 45
C41	−339 ± 11	−5260 ± 12	−2994 ± 14	1119 ± 62	1237 ± 11	−398 ± 12	−1865 ± 12	999 ± 55
O12	5392 ± 7	383 ± 7	−4401 ± 8	975 ± 35				
O13	5897 ± 8	1506 ± 8	−4285 ± 9	1134 ± 41				
C43	5531 ± 10	933 ± 11	−4763 ± 12	891 ± 49				
C44	5337 ± 10	1062 ± 11	−5724 ± 12	943 ± 52				
C45	6126 ± 19	1391 ± 21	−3292 ± 23	1807 ± 115				
C46	6542 ± 23	2020 ± 25	−2896 ± 28	2098 ± 145				
O14	1764 ± 17	−1329 ± 22	−8401 ± 21	2646 ± 132				
O15	2579 ± 10	−590 ± 10	−8777 ± 11	1441 ± 55				
C47	1879 ± 20	−717 ± 23	−8641 ± 22	1700 ± 110				
C48	1374 ± 26	−154 ± 27	−8780 ± 29	2293 ± 162				
C49	3143 ± 19	−1144 ± 19	−8638 ± 20	1653 ± 104				
C50	3876 ± 26	−873 ± 28	−8410 ± 30	2471 ± 182				
O16	1043 ± 19	5466 ± 20	−9086 ± 27	2916 ± 138				

TABLE 3

Compound SIII atomic coordinates (× 10^4) and equivalent isotropic thermal parameters (one third trace of the diagonalized matrix), with standard deviations

Atom	Molecule A				Molecule B			
	x/a	*y/b*	*z/c*	U_{eq} (× 10^4)	*x/a*	*y/b*	*z/c*	U_{eq} (× 10^4)
				$Å^2$				$Å^2$
S1	−4473 ± 2	−1671 ± 2	−1076 ± 5	829 ± 21	−5814 ± 2	−1856 ± 2	−3844 ± 5	830 ± 21
O1	−4802 ± 4	−1328 ± 4	−5388 ± 12	876 ± 58	−5503 ± 4	−1280 ± 4	345 ± 12	845 ± 55
O2	−4758 ± 4	−483 ± 4	−5995 ± 14	914 ± 59	−5375 ± 4	−412 ± 4	693 ± 12	859 ± 58
O3	−4300 ± 4	759 ± 4	−3512 ± 14	760 ± 57	−5643 ± 4	710 ± 4	−2311 ± 14	797 ± 58
O4	−4326 ± 5	181 ± 5	−773 ± 13	847 ± 62	−5730 ± 4	−21 ± 5	−4769 ± 14	850 ± 60
O5	−3805 ± 4	911 ± 4	−2030 ± 11	818 ± 36	−6167 ± 4	817 ± 4	−3761 ± 11	799 ± 35
O6	−2828 ± 4	27 ± 4	−3247 ± 11	806 ± 36	−7184 ± 3	96 ± 4	−2156 ± 11	754 ± 34
O7	−2318 ± 4	−757 ± 4	−1250 ± 11	808 ± 35	−7770 ± 4	−724 ± 4	−4027 ± 10	776 ± 34
O8	−1899 ± 5	−521 ± 6	−2702 ± 17	1335 ± 55	−8144 ± 5	−340 ± 5	−2647 ± 15	1135 ± 49
O9	−2308 ± 4	−1618 ± 4	−3423 ± 13	1071 ± 46	−7822 ± 4	−1527 ± 4	−1775 ± 12	932 ± 41
O10	−2827 ± 4	−2375 ± 5	−3952 ± 14	1156 ± 47	−7318 ± 4	−2244 ± 4	−998 ± 13	1087 ± 44
O11	−4095 ± 5	−2034 ± 5	−4806 ± 14	1233 ± 50	−5274 ± 4	−2467 ± 4	−2074 ± 11	871 ± 37
N1	−4671 ± 4	−2010 ± 5	−3629 ± 14	814 ± 65	−5746 ± 5	−2012 ± 4	−1071 ± 14	771 ± 60
N2	−4431 ± 4	−744 ± 5	−937 ± 15	630 ± 62	−5717 ± 5	−949 ± 5	−4362 ± 17	661 ± 67
N3	−4322 ± 5	−1139 ± 5	778 ± 19	894 ± 76	−5893 ± 5	−1413 ± 5	−5945 ± 17	851 ± 72
C1	−4694 ± 5	−1179 ± 6	−4355 ± 21	648 ± 83	−5559 ± 5	−1197 ± 6	−826 ± 20	648 ± 81
C2	−4634 ± 6	−1493 ± 5	−3419 ± 21	620 ± 81	−5662 ± 6	−1568 ± 6	−1579 ± 22	704 ± 85
C2′	−4403 ± 6	−1115 ± 8	−301 ± 23	767 ± 91	−5816 ± 6	−1364 ± 8	−4807 ± 22	766 ± 93
C3	−4547 ± 6	−1335 ± 6	−2326 ± 18	658 ± 78	−5684 ± 5	−1445 ± 5	−2669 ± 20	619 ± 81
C4	−4512 ± 5	−850 ± 5	−2108 ± 18	481 ± 69	−5644 ± 5	−1004 ± 6	−3146 ± 24	691 ± 92
C5	−4451 ± 5	17 ± 7	−2770 ± 25	810 ± 96	−5605 ± 5	−88 ± 6	−2724 ± 20	577 ± 73
C6	−4424 ± 5	288 ± 6	−3752 ± 29	780 ± 103	−5575 ± 6	257 ± 6	−1829 ± 25	721 ± 91
C7	−4539 ± 6	167 ± 7	−4847 ± 23	753 ± 93	−5477 ± 6	176 ± 7	−680 ± 23	760 ± 93
C8	−4642 ± 6	−333 ± 8	−5010 ± 20	703 ± 91	−5435 ± 6	−320 ± 7	−340 ± 22	727 ± 87
C9	−4617 ± 5	−684 ± 6	−4065 ± 19	578 ± 77	−5533 ± 5	−706 ± 6	−1272 ± 23	728 ± 89
C10	−4531 ± 5	−506 ± 6	−2979 ± 21	595 ± 79	−5587 ± 5	−612 ± 6	−2420 ± 19	607 ± 79
C11	−4343 ± 5	283 ± 7	−1776 ± 28	721 ± 96	−5684 ± 5	128 ± 7	−3788 ± 24	662 ± 86
C12	−4257 ± 6	781 ± 6	−2302 ± 22	746 ± 88	−5730 ± 5	667 ± 6	−3527 ± 24	803 ± 93
C13	−4523 ± 6	1188 ± 7	−1795 ± 18	946 ± 62	−5469 ± 6	1008 ± 6	−4199 ± 17	838 ± 58
C14	−4524 ± 6	497 ± 7	−5948 ± 19	918 ± 61	−5407 ± 6	595 ± 7	144 ± 17	850 ± 60
C15	−4397 ± 7	−2234 ± 7	−4240 ± 19	865 ± 63	−5536 ± 6	−2426 ± 7	−1327 ± 18	804 ± 56
C16	−4431 ± 6	−2801 ± 6	−4296 ± 16	746 ± 53	−5691 ± 6	−2868 ± 6	−630 ± 17	808 ± 57
C17	−4104 ± 7	−3083 ± 7	−4062 ± 21	1088 ± 70	−6086 ± 6	−3053 ± 6	−724 ± 16	771 ± 54
C18	−3722 ± 7	−2877 ± 8	−3518 ± 21	1163 ± 75	−6425 ± 5	−2889 ± 6	−1476 ± 15	712 ± 52
C19	−3387 ± 7	−3138 ± 7	−3130 ± 20	1091 ± 72	−6814 ± 5	−3069 ± 6	−1428 ± 16	712 ± 52
C20	−3002 ± 7	−2996 ± 7	−2558 ± 20	1011 ± 66	−7158 ± 6	−2938 ± 6	−2212 ± 18	885 ± 61
C21	−2914 ± 6	−2440 ± 7	−2753 ± 19	858 ± 59	−7260 ± 5	−2376 ± 5	−2181 ± 16	690 ± 50
C22	−2508 ± 6	−2285 ± 6	−2116 ± 18	869 ± 60	−7650 ± 6	−2230 ± 6	−2947 ± 17	814 ± 55
C23	−2396 ± 6	−1741 ± 7	−2212 ± 18	863 ± 58	−7733 ± 6	−1671 ± 6	−2912 ± 18	827 ± 56
C24	−2773 ± 5	−1425 ± 6	−1867 ± 16	679 ± 50	−7334 ± 5	−1384 ± 6	−3282 ± 15	665 ± 49
C25	−2675 ± 5	−879 ± 5	−2056 ± 15	670 ± 49	−7430 ± 5	−839 ± 5	−3205 ± 15	625 ± 48
C26	−3028 ± 5	−519 ± 5	−1715 ± 14	573 ± 46	−7052 ± 5	−521 ± 5	−3615 ± 15	668 ± 49
C27	−2903 ± 5	5 ± 6	−2089 ± 17	729 ± 52	−7145 ± 5	26 ± 6	−3366 ± 15	619 ± 48
C28	−3250 ± 6	354 ± 6	−1626 ± 17	809 ± 58	−6775 ± 5	332 ± 6	−3923 ± 16	717 ± 51
C29	−3507 ± 6	564 ± 6	−2438 ± 17	756 ± 54	−6487 ± 5	528 ± 6	−3201 ± 15	664 ± 50
C30	−4859 ± 7	−2943 ± 7	−4805 ± 20	1093 ± 72	−5338 ± 7	−3063 ± 7	141 ± 20	1153 ± 76
C31	−3046 ± 8	−3105 ± 8	−1277 ± 24	1366 ± 87	−7086 ± 8	−3120 ± 8	−3463 ± 24	1401 ± 94
C32	−2073 ± 7	−2580 ± 8	−2560 ± 23	1303 ± 83	−8083 ± 7	−2499 ± 7	−2539 ± 20	1095 ± 72
C33	−2914 ± 6	−1508 ± 7	−567 ± 20	1031 ± 71	−7204 ± 7	−1508 ± 7	−4542 ± 20	1029 ± 71
C34	−3447 ± 6	−659 ± 7	−2401 ± 17	899 ± 60	−6653 ± 7	−682 ± 7	−2845 ± 20	1103 ± 72
C35	−1929 ± 7	−572 ± 7	−1729 ± 21	915 ± 65	−8126 ± 7	−460 ± 7	−3548 ± 22	932 ± 66
C36	−1614 ± 8	−495 ± 9	−822 ± 23	1364 ± 89	−8436 ± 8	−425 ± 8	−4570 ± 22	1260 ± 83
C37	−2523 ± 8	389 ± 9	−3513 ± 23	1455 ± 95	−7443 ± 6	520 ± 7	−1950 ± 18	970 ± 65
C38	−4273 ± 7	−664 ± 8	1463 ± 20	1115 ± 75	−5872 ± 7	−1009 ± 8	−6717 ± 19	1007 ± 68
C39	−3783 ± 7	−460 ± 7	1287 ± 20	1162 ± 74	−6304 ± 7	−714 ± 8	−6682 ± 20	1162 ± 76
C40	−4154 ± 11	−1628 ± 12	1432 ± 31	1874 ± 129	−6035 ± 7	−1925 ± 8	−6403 ± 21	1166 ± 76
C41	−4559 ± 16	−1693 ± 16	1796 ± 39	2638 ± 205	−5646 ± 8	−2137 ± 9	−7069 ± 24	1493 ± 97
O12	−6575 ± 5	−1828 ± 6	119 ± 16	1707 ± 66				
C42	−6613 ± 14	−1246 ± 16	169 ± 38	2611 ± 188				
C43	−6948 ± 16	−1130 ± 17	391 ± 44	2973 ± 231				
O13	−1333 ± 14	−1670 ± 15	−3818 ± 38	3999 ± 203				
C44	−792 ± 24	−1366 ± 27	−3467 ± 70	4683 ± 423				
C45	−1175 ± 28	−1122 ± 29	−3737 ± 78	5037 ± 490				
O14	−5944 ± 8	530 ± 8	−6790 ± 22	2684 ± 109				
O15	−5255 ± 11	107 ± 12	−7416 ± 28	1663 ± 122				

upon thermomicroscopic observation, but the DSC heating curve shows several endo-exothermic events in a broad range of temperatures, leading to a product that decomposes at 230°. This behavior is typical of a mixture of different polymorphic forms. From several crystallization trials the following polymorphic forms have now been isolated; their physical properties are reported in Table 4.

Form I was obtained by the heating of form II at 180° after recrystallization of the melt. The DSC heating curve (Fig. 2, *curve 1a*) shows a sharp endothermic peak at 230–238° due to melting immediately followed by decomposition. In microscopy, this form shows birefringence and a poorly defined morphology. In the temperature range of 25–120° desolvation of imbibition water is recorded, which corresponds to 2% weight loss (Fig. 2, *curve 1b*). In Fig. 3a, the FT-IR spectrum of form I is reported. The relatively high melting point might be associated with a strong packing that could be the consequence of a suitable conformation of the acetyl group, as shown in rifampicin polymorphism (12). The X-ray powder diffraction data are reported in Table 5; the presence of the amorphous phase is indicated by the background values and is due to the possible decrease of crystallinity degree caused by thermal treatment.

Form II, isolated by crystallization of rifamexil from 95% ethanol, shows birefringence in microscopy with polarized light and in DSC analysis shows the thermal profile reported in Fig. 2, *curve 2a*. An endothermic peak at 180–185° corresponds to the melting of form II followed by an exothermic event (190°) due to recrystallization into form I. In the temperature range of 25–120°, desolvation of imbibition water occurs. The transformation of form II into form I does not occur when the melting point is determined in capillary tubes or by thermomicroscopy, because the oxygen of air catalyzes the decomposition of the product. The IR spectrum is reported in Fig. 3b; the X-ray powder diffraction pattern, which is given in Table 5, is characteristic of a crystalline powder with a relatively high degree of crystallinity.

The amorphous form, obtained by grinding of form I, form II, and solvates or by rapid evaporation of a chloroform solution, shows the heating curve reported in Fig. 2, *curve 3a*. Only a change in specific heat in the temperature range of 160–170° is recorded, followed by decomposition. A broad endotherm in the temperature range of 25–130°, which is associated with weight loss, is due to desolvation of imbibition water. In microscopy with polarized light it does not show birefringence. In Fig. 3c the IR spectrum is reported.

Solvate SI was obtained by the heating at 60° of a crystalline powder of rifamexil crystallized from ethyl acetate solution. In microscopy it shows birefringence, and in DSC analysis the thermal profile reported in Fig. 4, *curve 1a*, was obtained. An endothermic peak at 165–170°, due to melting and desolvation of 1 mol of ethyl acetate, is followed by decomposition. Between 25 and 110°, a broad endotherm due to desolvation of imbibition water is recorded. By TG (Fig. 4, *curve 1b*), two weight losses are recorded. The first, between 25 and 110°, is due to imbibition water and the second, at 130–170° (about 2%), is due to the desolvation of ethyl acetate. The IR spectrum of SI is reported in Fig. 3d, whereas the X-ray powder data are in Table 5. The X-ray pattern is characteristic of a crystalline powder, although the appearance of the background values is indicative of the presence of an amorphous phase as well.

Solvate SII, isolated from ethyl acetate solution after a very slow crystallization process at room temperature, shows birefringence in microscopy with polarized light. The DSC heating curve (Fig. 4, *curve 2a*) shows a sharp peak at 153°, followed by decomposition. A second endotherm at 147°, immediately before the highest one, is well correlated by the TG curve (Fig. 4, *curve 2b*). In fact, two different weight losses are recorded; the first, between 50 and 150° (about 7%), is followed by the second, at 150–170°, with a weight loss of 6%. This thermal behavior indicates that two molecules of ethyl acetate are present in the lattice, interacting in different ways with the two rifamexil molecules. The first solvent molecule is lost easily at relatively low temperature, whereas the second one is more strongly bonded to rifamexil and needs more energy to be removed. The lattice of SII is rather unstable and loses part of the solvent when it is exposed to air at ambient conditions, becoming amorphous. Because of physical instability, it was not possible to record IR and X-ray powder spectra. Nevertheless, a single-crystal X-ray determination was carried out by protecting the crystal in a Lindemann capillary (see above).

Solvate SIII was obtained by very slow crystallization of a solution of rifamexil in 95% ethanol at room temperature. In microscopy it shows birefringence and by heating (DSC) a broad endotherm in the temperature range of 25–160°, with peaks at 110° and 125°, is recorded (Fig. 4, *curve 3b*). This event is due to the desolvation of ethanol of crystallization (8%), during which several modifications occur. In fact, at 180°, 190°, and 230° endothermic and exothermic transitions due to melting and crystallization of polymorphic forms (II

TABLE 4
Polymorphic forms of rifamexil

Form or solvate	Melting point or transition temperature	Crystallization solvent	Weight loss[a]	Stoichiometry	Subsequent events
			%		
I	238°				Decomposes
II	185°				Transforms into form I
SI[b]	165–170°	Ethyl acetate	~2	~0.5	Decomposes
SII[c]	120–160°	Ethyl acetate/water	~13	1 ethyl acetate + 0.5 water	Decomposes
SIII[c]	30–160°	Ethanol/water	~8	1 ethanol + 1 water	Transforms into form II and then into form I
Amorphous	160–170°				Decomposes

[a] In addition, all forms and solvates contain ~2% imbibition water.
[b] Obtained from partial desolvation of SII. Until now it has never been isolated as a pure crystalline phase.
[c] Stoichiometry obtained from X-ray structure determination.

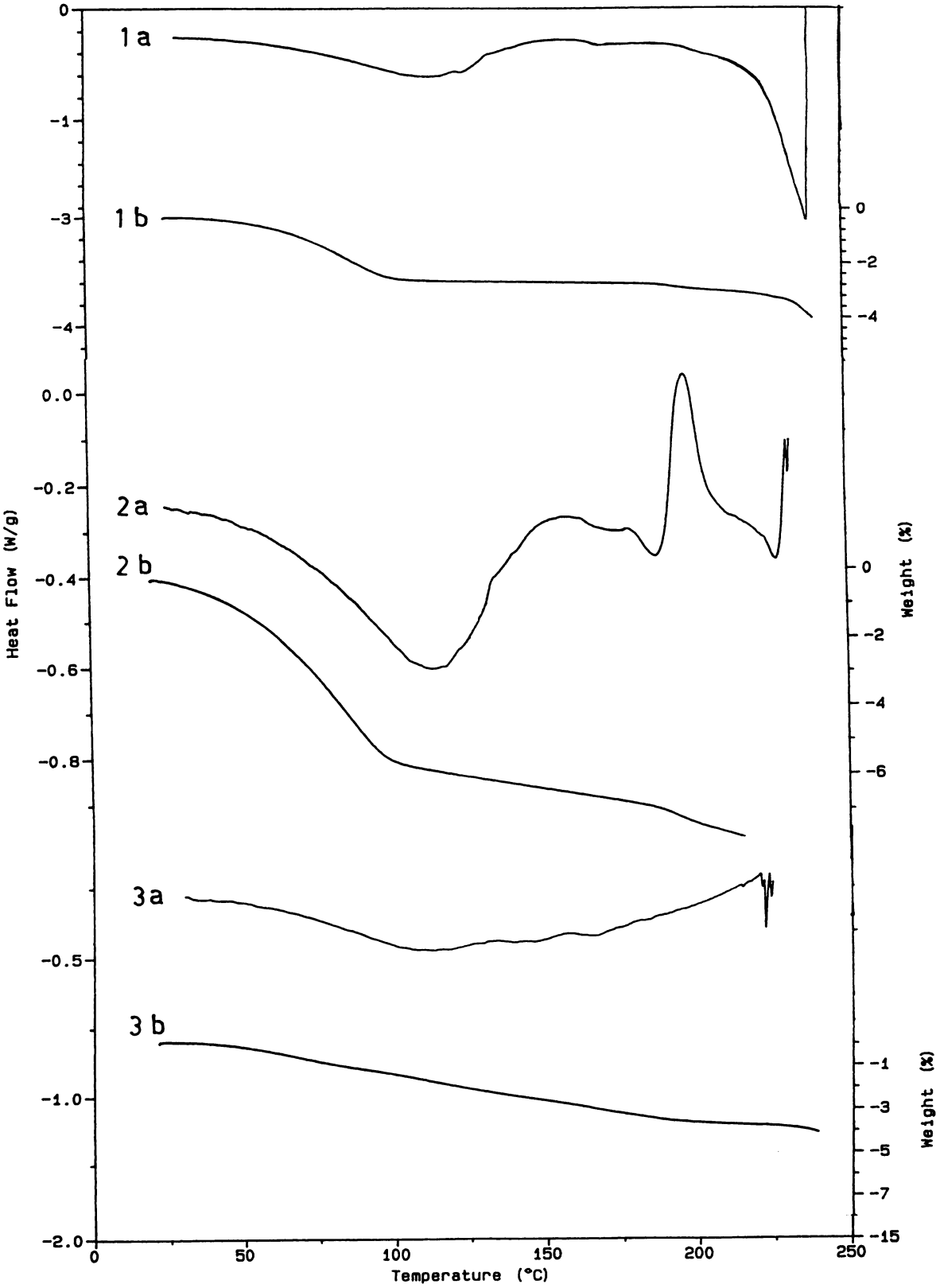

Fig. 2. DSC (a) and TG (b) heating curves. *1*, Form I; *2*, form II; *3*, amorphous form.

and I) are recorded. This solvate is very unstable and loses the crystallization solvents when exposed to ambient conditions, becoming amorphous. Physical instability prevented the recording of IR and X-ray powder spectra. However, in this case as well, a single-crystal X-ray analysis was made possible by protecting the crystal in a Lindemann capillary.

X-ray crystal structures of solvates SII and SIII. The two compounds are very similar in the overall conformation

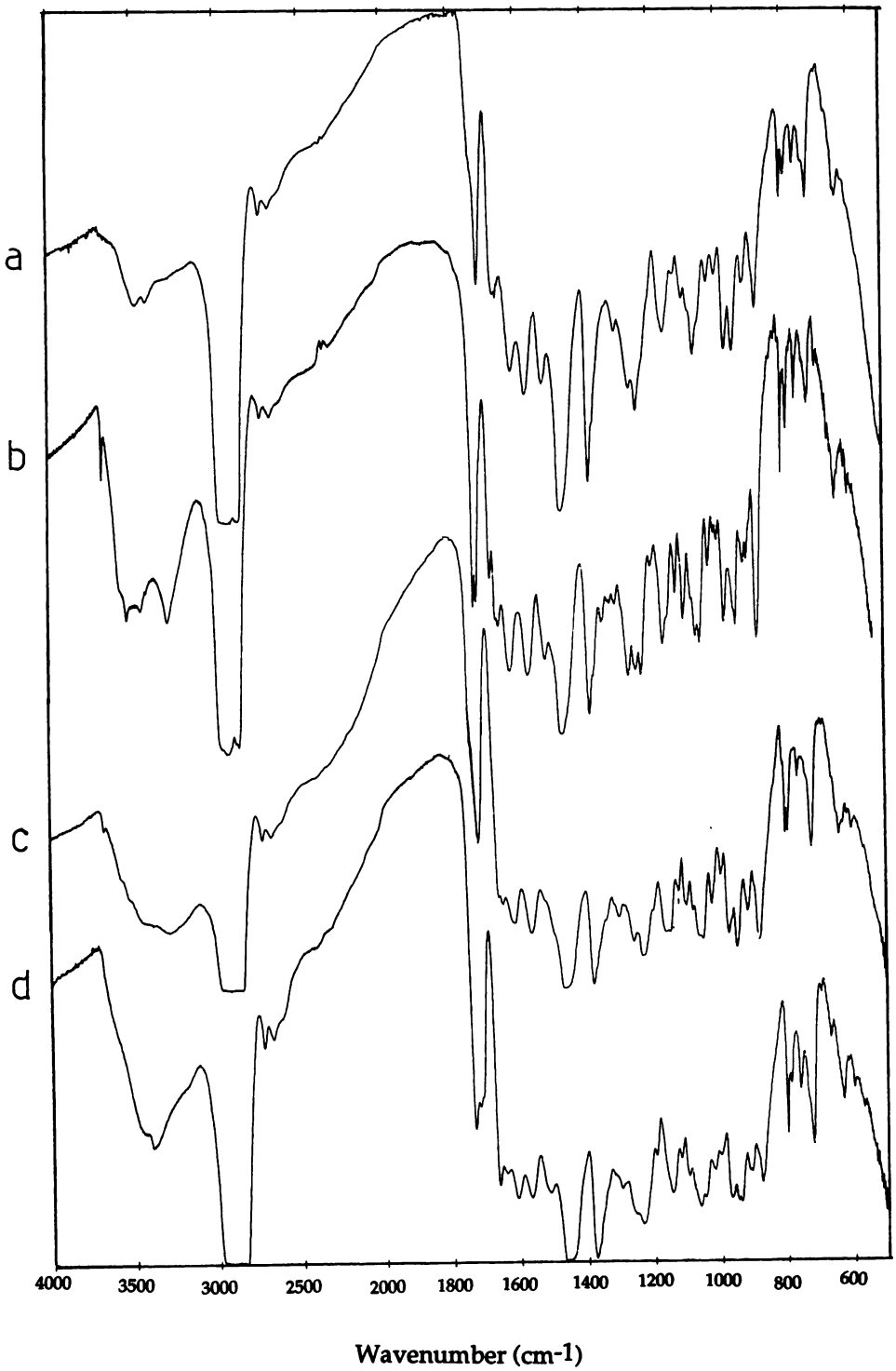

Fig. 3. FT-IR spectra (Nujol mull). a, Form I; b, form II; c, amorphous material; d, SI.

of the rifamexil molecule, as well as in the fact that in each case the two independent molecules (A and B) are paired by strong hydrogen bonds, but they differ basically in the mutual orientation of these molecules as a consequence of the different hydrogen-bonding networks; moreover, in SIII molecules A and B are arranged to interact also through π-π contacts between the hydroquinone nuclei, whereas this is not possible in SII because of the different packing motif. It must be pointed out that the X-ray analysis leaves no doubt as to the presence of the hydrogen-bonding in the crystal packing of both compounds, although, as mentioned in Materials and Methods, none of the hydrogen atoms could be located in the difference maps. In fact, a careful examination of the interatomic contacts reveals that the shortest ones can be certainly considered as hydrogen bonds, because their values all fall in the expected range (23, 24). ORTEP views of the rifamexil molecule in the two compounds are shown in Figs. 5 and 6 (the drawing refers in both cases to molecule A). Comparison of the geometries of rifamexil in the two compounds indicates that the structural parameters in the four

TABLE 5
X-ray powder diffraction data[a]

Form I		Form II		SI	
d	I/I_{max}	*d*	I/I_{max}	*d*	I/I_{max}
Å		Å		Å	
26.39	5.54	14.57	13.63	13.79	33.41
12.03	25.74	12.32	3.32	13.53	39.53
10.52	36.35	9.97	100.00	12.09	100.00
9.58	24.27	9.52	2.83	10.50	67.46
7.34	21.46	8.03	5.90	10.22	24.93
6.95	14.62	7.40	29.38	10.03	26.50
6.17	40.92	6.80	3.67	9.15	29.98
5.78	26.49	5.90	6.73	8.56	37.18
5.61	38.15	5.36	16.15	8.43	40.37
5.13	100.00	5.05	60.90	6.99	25.18
4.68	24.27	4.96	82.18	6.80	36.94
4.36	14.62	4.67	3.15	6.22	35.86
3.85	60.75	4.52	13.80	6.00	30.42
3.70	37.25	4.33	3.76	5.97	32.63
3.04	20.12	4.18	1.59	5.79	30.76
		4.08	3.67	5.70	28.61
		3.96	12.45	5.57	31.50
		3.72	89.54	5.39	26.55
		3.63	6.49	5.20	35.71
		3.53	13.46	5.07	31.11
		3.48	5.46	4.88	26.26
		3.36	7.47	4.68	38.02
		3.23	3.41	4.55	28.80
		3.18	8.13	4.40	29.15
		3.05	3.67	4.15	29.83
		2.98	17.49	4.03	33.36
		2.88	3.49	3.84	24.93
		2.79	1.16	3.81	22.39
		2.70	3.85	3.60	23.17
		2.64	1.90	3.35	23.22
		2.62	1.90	3.29	19.79
		2.50	1.97		
		2.18	1.77		

[a] d = distance, Å = unit of measure.

independent molecules agree reasonably well. A full listing of bond distances and angles is available from the authors on request.

Previous studies aimed at investigating the structure-activity relationships for rifamycins (8, 15) have indicated the following basic requirements for biological activity, all of which are fulfilled in our compounds: (i) a naphthalene ring carrying oxygen atoms at C1 and C8, in either the quinone or the hydroquinone form, (ii) two free hydroxyl groups at C21 and C23 in the ansa chain, and (iii) a well defined spatial arrangement of oxygen atoms at C21 and C23. The rifamexil molecule, as a whole, is made up of a nearly planar part, formed by the naphthohydroquinone nucleus and the two five-membered rings condensed to it, and a 17-membered ansa chain that is connected to C2 and C12. The maximum displacement of any atom from the best plane defined by the 16 atoms of the four fused rings is about 0.20 Å. The 17 atoms of the ansa-chain skeleton define a plane to within 0.5 Å in each case. The dihedral angles between this plane and that containing the chromophore are 75.1 ± 2° (molecule A) and 100.7 ± 2° (molecule B) in SII and 64.3 ± 3° (molecule A) and 64.7 ± 3° (molecule B) in SIII. In the active rifamycins this angle lies in the rather narrow range of 71–123°, indicating somewhat similar overall conformations of the molecules. The three-dimensional arrangement of the oxygen atoms O1, O2, O9, and O10 shows a common pattern in all active rifamycins. The distances among these atoms in our compounds are as follows: O1–O2, 2.41–2.47 Å; O9–O10, 2.69–2.76 Å; O1–O10, 5.48–7.03 Å; O1–O9, 6.81–8.18 Å; O2–O10, 6.81–8.34 Å; O2–O9, 7.35–8.81 Å. The four oxygen atoms all lie on the same side with respect to the ansa-chain best plane, with the C21-O10 and C23-O9 bonds being nearly perpendicular to the plane. Of the remaining eight substituents of the ansa chain, four, i.e., the methyl groups on C30, C32, and C34 and the methoxyl group at C27, are on the same side of the aforementioned atoms and three, i.e., the methyl groups on C31 and C33 and the acetoxyl group at C25, are displaced in the opposite direction, whereas the carbonyl oxygen O11 lies on the same side of the four oxygens in both molecules of SII and in molecule B of SIII and is on the opposite side in molecule A of SIII, indicating a discrete flexibility for the amidic group containing O11. The conformation of this group can be characterized by analysis of the geometry of the ring/chain junctions; the relative torsion angles for C1-C2-N1-C15 (τ_1) and N1-C15-C16-C17 (τ_2) at the amidic junction and C26-C27-C28-C29 (τ_3) and C28-C29-O5-C12 (τ_4) at the O5-C12 junction are shown in Table 6. As can be seen by the values of τ_1 and τ_2, the amidic group of molecule A of SIII shows a conformation opposite to that of the other three molecules, as a consequence of the hydrogen bond between the amidic nitrogen N1 (in molecule A) and the carbonyl oxygen O11 (in molecule B) (see below). This behavior of the amidic group of the same active rifamycin molecule involved in different packing environments suggests a certain degree of conformational freedom of the amidic junction, so that its geometry cannot be directly correlated with the pharmacological properties of the compounds (25, 26).

Each independent molecule in both SII and SIII is involved in three intramolecular hydrogen bonds, which occur between O1 and O2 (2.41–2.47 Å), O9 and O10 (2.69–2.76 Å), and N2 and O4 (2.59–2.64 Å). Within each compound the molecules A and B are connected by intermolecular hydrogen bonds, although in different manners, as shown in Figs. 7 and 8, which also emphasize the different mutual orientation of the two independent molecules in the two compounds. In both structures, each molecule A is hydrogen-bonded to a molecule B in such a way that dimeric rifamexil units are formed. Nevertheless, whereas the carbonyl oxygen O11 of molecule B is an acceptor in both cases, the donor is the hydroxyl oxygen O10 in SII and the amidic nitrogen N1 in SIII, with both donors belonging to molecule A [SII: O10 (molecule A)–O11 (molecule B), 2.81 ± 1 Å; SIII: N1 (molecule A)–O11 (molecule B), 2.90 ± 2 Å]. Another important difference between the two compounds concerns the role of the solvent molecules in the molecular packing, which is shown in Figs. 9 and 10. In SII one of the two ethyl acetate molecules is involved in a hydrogen bond with the hydroxyl oxygen O10 of molecule B (O12–O10, 2.99 ± 1 Å), whereas, rather uncommonly, the other ethyl acetate and the water molecule do not participate in any contact of <3.5 Å, in agreement with their high thermal parameters and with the results of TG analysis. In SIII one of the ethanol molecules is interposed between the N1 and O10 atoms of molecule B through hydrogen bonds (O12–N1, 2.99 ± 2 Å; O12–O10, 2.90 ± 2 Å), whereas the second molecule is involved in only one, rather weak, interaction with the O9 atom of molecule A (O13· · ·O9, 3.09 ± 4 Å). Both of the water molecules are hydrogen-bonded to the rifamexil molecules. O14 acts as

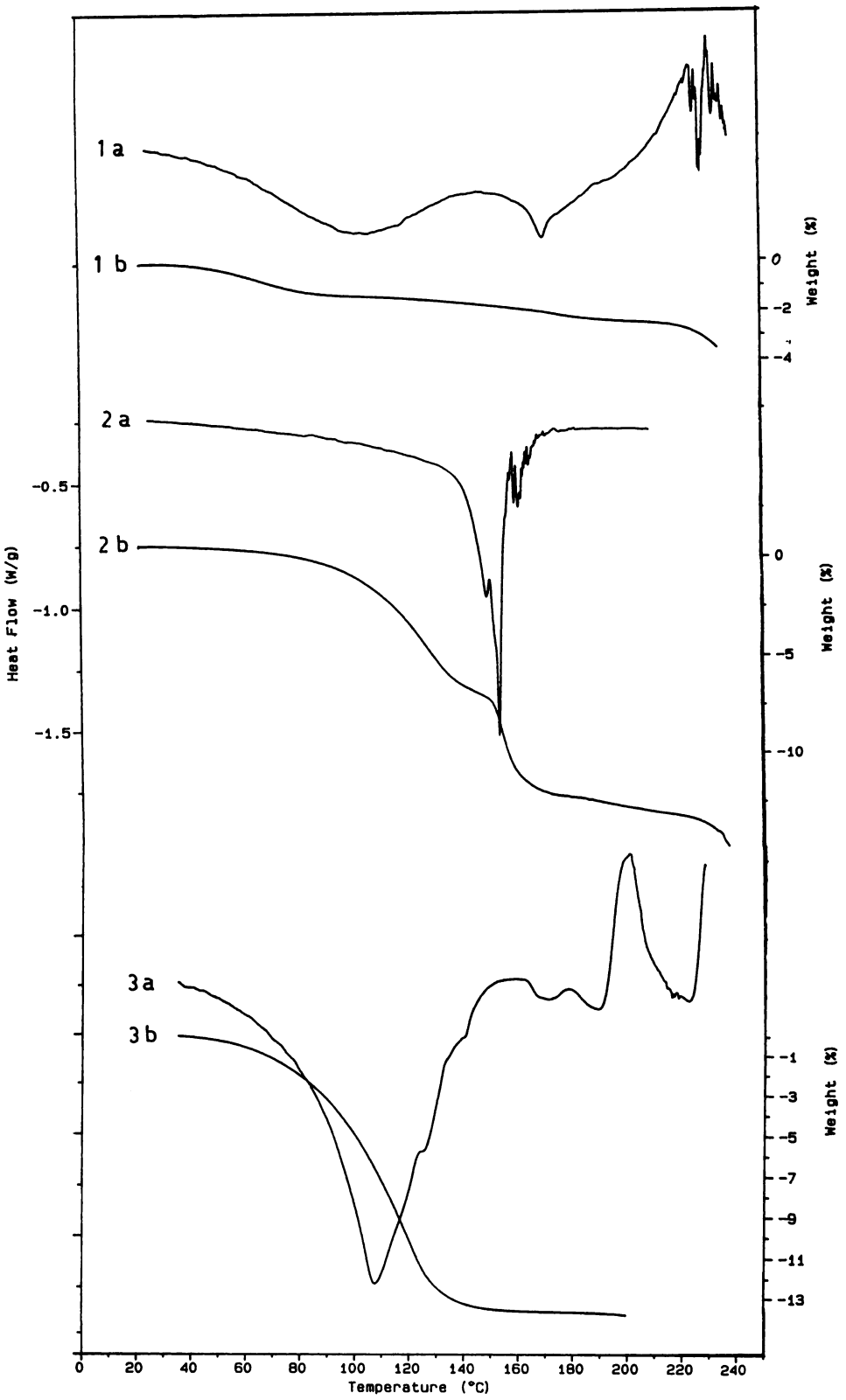

Fig. 4. DSC (a) and TG (b) heating curves. *1*, SI; *2*, SII; *3*, SIII.

donor towards O4 (molecule B) (2.88 ± 3 Å) and O15 (2.56 ± 4 Å). In addition to acting as an acceptor in the aforementioned hydrogen bond, O15 uses its own hydrogens to bridge molecule A at x,y,z and molecule B at $x,y,z-1$, through the O15–O2 (molecule A) (2.80 ± 4 Å) and O15–O2 (molecule B^i) (2.65 ± 4 Å) hydrogen bonds. In both compounds pairs of molecules A and B face one another through the aromatic moieties, which make angles of 2.5 ± 3° in SII and 4.2 ± 3° in SIII, with the minimum distance being C1 (molecule A)–C5 (molecule B^i) (3.33 ± 2 Å) ($i = -x,y+½,-z$) and C1

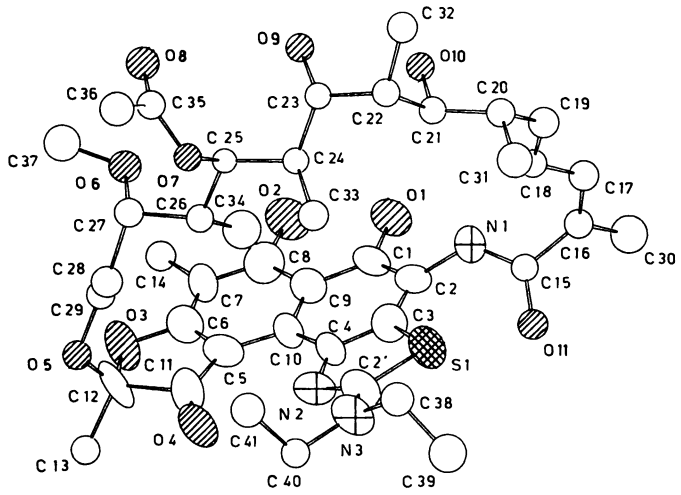

Fig. 5. ORTEP view of rifamexil (molecule A) in SII. Thermal ellipsoids are drawn at the 50% probability level.

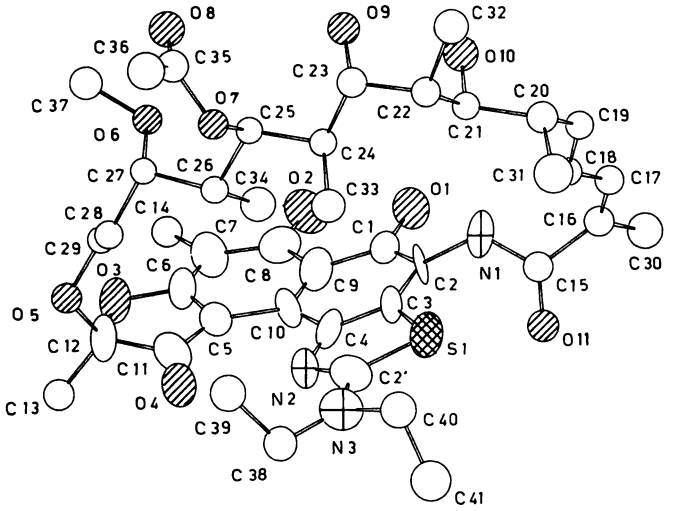

Fig. 6. ORTEP view of rifamexil (molecule A) in SIII. Thermal ellipsoids are drawn at the 50% probability level.

TABLE 6
Torsion angles

	Angle			
	SII Molecule A	SII Molecule B	SIII Molecule A	SIII Molecule B
	degrees			
τ_1	−149 ± 1	−141 ± 1	68 ± 2	−123 ± 2
τ_2	70 ± 2	65 ± 2	−127 ± 2	65 ± 2
τ_3	−98 ± 2	−100 ± 2	−111 ± 2	−106 ± 2
τ_4	−130 ± 2	−100 ± 2	−121 ± 2	−124 ± 2

(molecule A)–C4 (molecule B) (3.33 ± 3 Å), respectively. Whereas in SII the two hydroquinone nuclei are tilted and the lines C2 (molecule A)–C6 (molecule A) and C2 (molecule B^i)–C6 (molecule B^i) form an angle of 100.1 ± 3°, in SIII the two aromatic moieties of molecule A and B are almost parallel and the two C2–C6 (molecules A and B) lines form an angle of 4.6 ± 4°. So, in addition to the hydrogen bonds described above, a π-π interaction (27) locking together molecules A and B is possible in SIII and not in SII. In summary, the packings in the crystal structures of the polymorphs SII and SIII differ in the following respects: (i) the nature of the

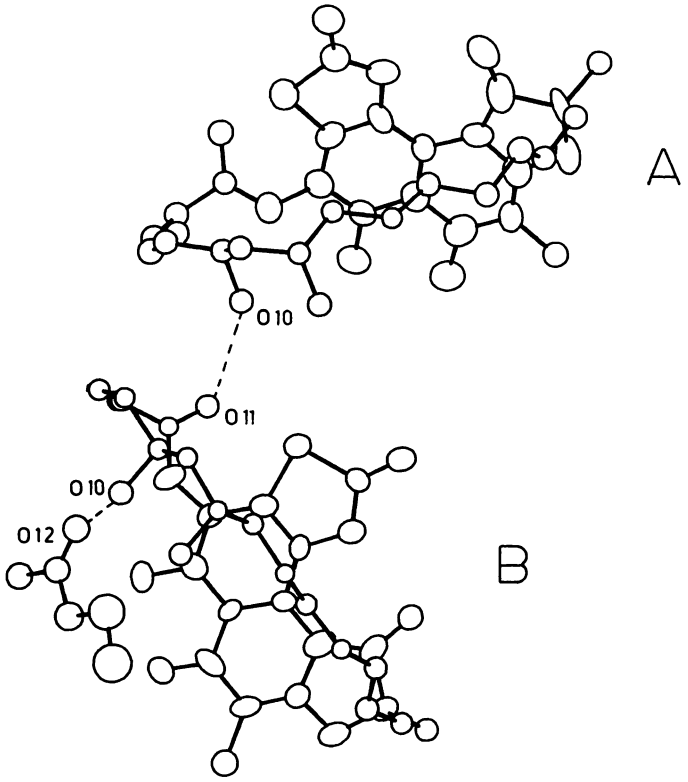

Fig. 7. Crystal packing in SII, showing dimeric rifamexil units and solvent molecule-rifamexil interactions.

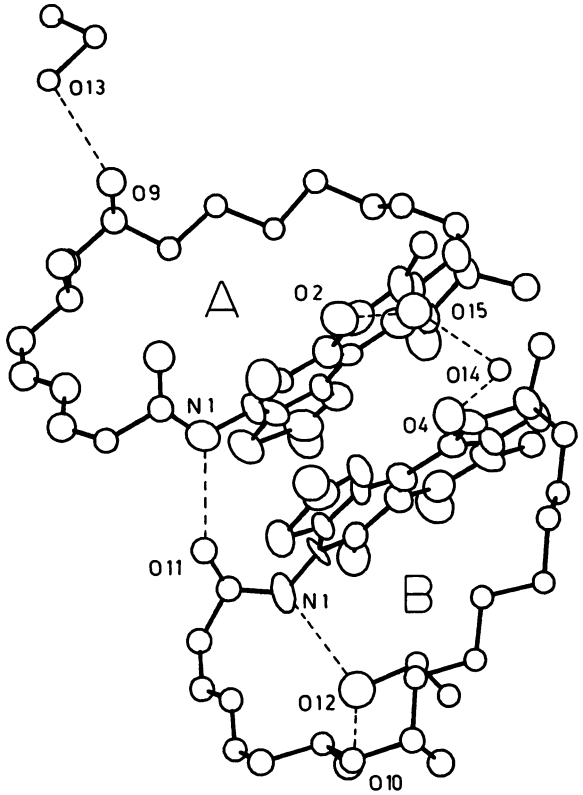

Fig. 8. Crystal packing in SIII, showing dimeric rifamexil units and solvent molecule-rifamexil interactions.

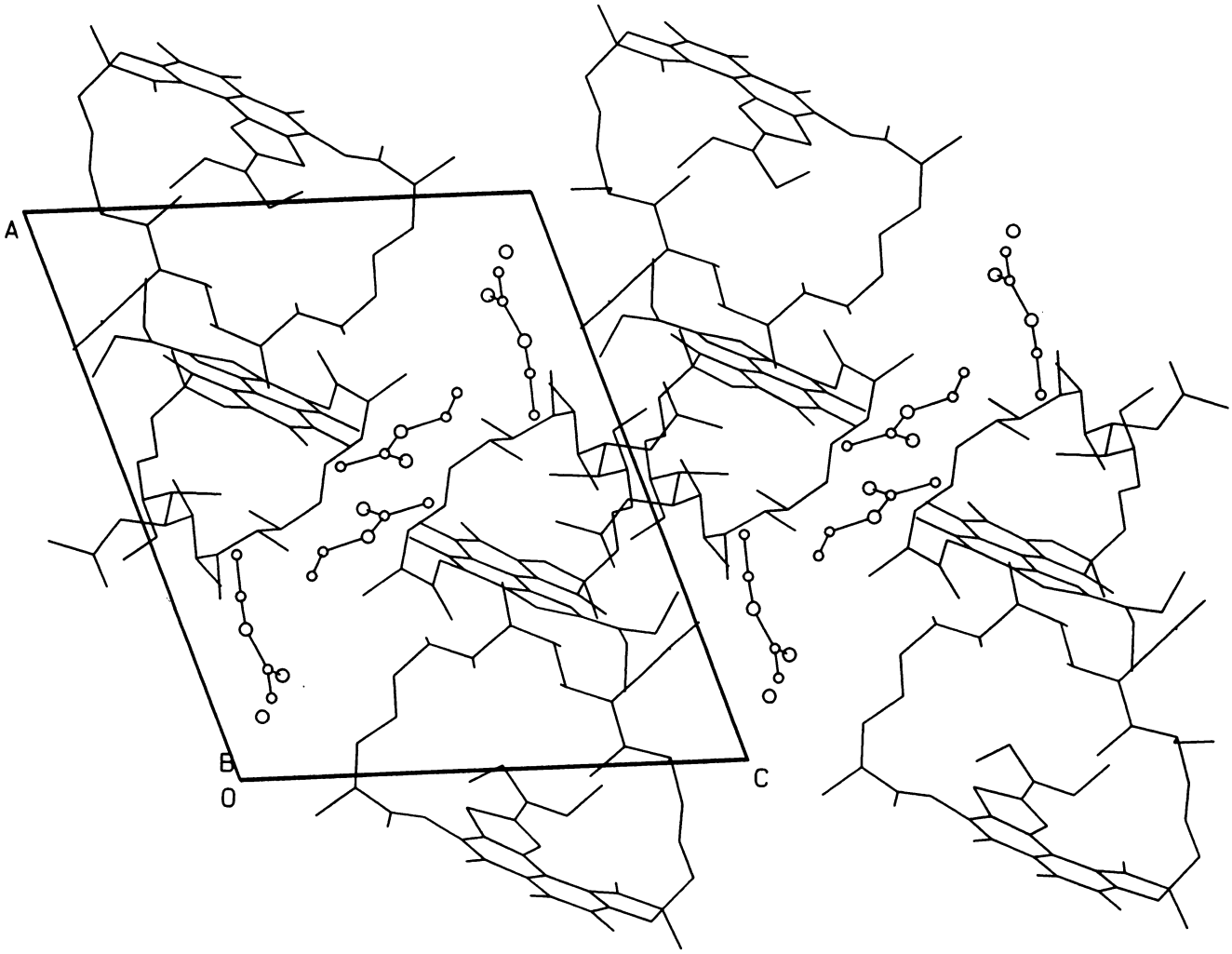

Fig. 9. Packing diagram for SII.

donor atoms in the hydrogen bonds that give rise to the dimeric rifamexil units, which causes a different mutual orientation of molecules A and B in the two compounds, (ii) the interactions between rifamexil and solvent molecules, in agreement with the different thermal behavior of the two forms, and (iii) the π-π interactions between the chromophore nuclei of molecules A and B that are present only in SIII, thus justifying its highly thermal stability.

Statistical analysis of activity and structural parameters. To determine a more general criterion correlating structural data with biological activity, a multivariate statistical analysis has been undertaken on the 24 rifamycin molecules structurally characterized up to now, i.e., sodium rifamycin SV (26) (**a**),[1] 21-acetoxy-(11*R*)-rifamycinol S (28) (**b**), 3-methoxycarbonylrifamycin S (25) (**c**), rifamycinol (29) (**d** and **e**), (11*R*)-25-*O*-deacetyl-11-deoxo-11-hydroxy-21,23-*O*-isopropylidene rifamycin S (30) (**f**), rifamycin P (31) (**g** and **h**), rifampicin (32) (**i**), rifamycin B *p*-iodoanilide (8) (**l**), rifamycin Y *p*-iodoanilide (8) (**m**), rifamycin S iminomethyl ether (33) (**n** and **o**), tolypomycinone (34) (**p**), SII (**q** and **r**) and SIII (**s** and **t**) (this work), 4-deoxy-3′-bromopyrido[1′,2′,1,2]imidazo[5,4-*c*]rifamycin S (35) (**u**), monoclinic rifamycin S (16) (**v**), 25-*O*-deacetyl-27,28-didehydro-27-demethoxy-11-deoxo-11,29-epoxy-28,29-dihydro-21,23-*O*-isopropylidenrifamycin S (36) (**w** and **y**), orthorhombic rifamycin S (15) (**x**), and cyclized rifamycin SV (11) (**z**). Calculations were performed using STATGRAPHICS (Manugistics, Rockville, MD) and SAS (SAS Institute, Cary, NC) software. The structural parameters were retrieved using the October 1993 release of the Cambridge Crystallographic Database. Initially 26 structural parameters, comprising torsion angles,[2] interatomic distances, and angles between planes, were selected to represent the molecular conformations of active and nonactive rifamycins (Table 7). The correlation matrix of all 26 variables was considered, and 16 parameters were discarded among the most correlated ones. A PCA was then performed on the remaining variables, and the resulting scatter plot on PC1 and PC2 of the 24 rifamycins showed a separation between active and nonactive molecules. After the three variables with lowest loadings on PC1 and PC2 were discarded, the PCA gave substantially the same scatter plot. This is shown in Fig. 11b. The values of the means and standard deviations used to standardize the seven variables are reported in Table 7. The eigenvalues quickly fall off after the

[1] The letters identify the compounds in Fig. 11b.

[2] Torsion angles T2, T5, T6, T8, T9, T11, T12, T13, T14, and T16 have values falling close to ±180°. To perform a meaningful statistical analysis it was necesssary to express them in the range of 0–360° (37).

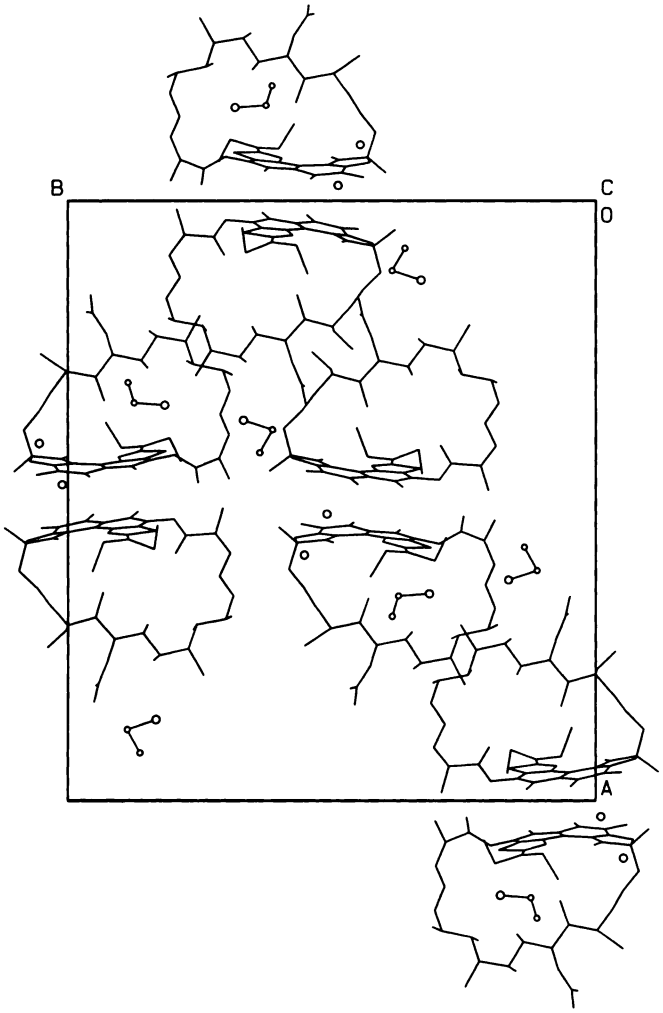

Fig. 10. Packing diagram for SIII.

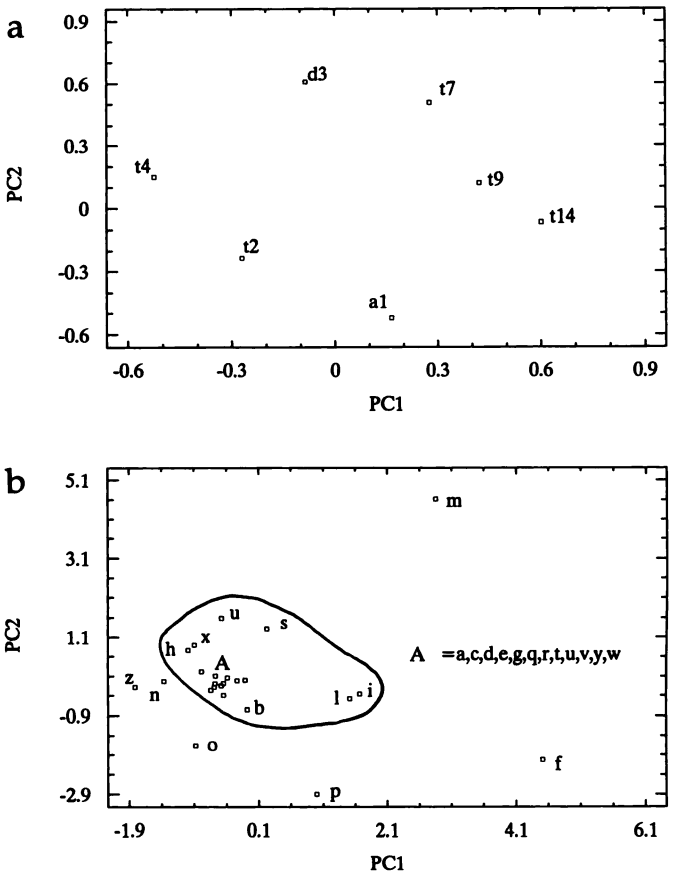

Fig. 11. Results of the PCA. a, Loadings of the seven variables on PC1 and PC2; b, scatter plot of PC1 versus PC2 for the 24 rifamycin molecules. Active compounds lie within the contoured area.

first two components, indicating that a model based on PC1 and PC2 should be examined. The first two PCs account for 55% of the total variance. The scatter plot of PC1 versus PC2 shows that in the PC1/PC2 space all of the active rifamycin molecules cluster together in a group, whereas all of the nonactive compounds fall outside this area, showing that the discriminant power arises from both PC1 and PC2. Even if the model based on PCA succeeds in separating the compounds on the basis of their activity, the discrimination between the two groups is not straightforward, as shown by the shape of the area containing the active compounds. Another pattern is obtained by DF analysis by considering the seven variables described above. Both the classification power and the prediction power calculated by cross-validation are 87.5%. The same results were obtained by reducing the number of variables to four, discarding the less significant ones. Misclassified compounds are **i**, **l**, and **m**. The relationship for the DF with four standardized variables is DF = 0.326T2 −

TABLE 7

Structural parameters considered in the statistical analysis

The seven parameters selected for the PCA are indicated, along with the mean and standard deviation values used to standardize them.

Parameter[a]	Value	Parameter	Value
A1 = p Λ C21-O10[b]	85.74 ± 33.2	T11 = t C23-C24-C25-C26	
A2 = p Λ C23-O9		T12 = t C24-C25-C26-C27	
A3 = p Λ ansa		T13 = t C25-C26-C27-C28	
T1 = t C2-N1-C15-C16		T14 = t C26-C27-C28-C29[b]	−67.63 ± 99.0
T2 = t N1-C15-C16-C17[b]	43.90 ± 73.0	T15 = t C27-C28-C29-O5	
T3 = t C15-C16-C17-C18		T16 = t C28-C29-O5-C12	
T4 = t C16-C17-C18-C19[b]	176.11 ± 29.2	T17 = t C29-O5-C12-O3	
T5 = t C17-C18-C19-C20		D1 = d O1···O2	
T6 = t C18-C19-C20-C21		D2 = d O1···O9	
T7 = t C19-C20-C21-C22[b]	184.22 ± 22.0	D3 = d O1···O10[b]	5.73 ± 1.2
T8 = t C20-C21-C22-C23		D4 = d O2···O9	
T9 = t C21-C22-C23-C24[b]	48.63 ± 63.6	D5 = d O2···O10	
T10 = t C22-C23-C24-C25		D6 = d O9···O10	

[a] p, naphthohydroquinone plane; ansa, average plane of the ansa chain, Λ, angle; t, torsion angle; d, distance.
[b] Used for PCA.

0.509T9 + 0.910T14 − 0.680D3 (p = 2.6% with exact F statistics). The class mean values of DF are −0.475 for active compounds and 1.426 for nonactive compounds. By examining the loadings relative to the different variables resulting by both PC (Fig. 11a) and DF analyses, it can be seen that the most effective geometric parameters in determining the separation between active and nonactive compounds are those related to the conformation of the C21–C27 segment of the ansa chain and to the relative orientation of the C21–O9 and C23–O10 vectors with respect to the naphthoquinone plane.

The statistical analysis indicates the geometric parameters that mainly contribute to differentiating the conformations of active and nonactive rifamycins and provides a quantitative tool to predict the activity of rifamycins on the basis of their molecular geometry. The discriminant power has been shown to be mainly determined by the geometry of the C21–C27 segment of the ansa chain and by the spatial arrangement of the O1, O2, O9, and O10 atoms. These results are consistent with the qualitative requirements for activity indicated in the literature on rifamycins. Moreover, they support our hypothesis that the conformation of the amidic junction is not one of the major factors that affects the activity of the molecule.

Acknowledgments

We gratefully acknowledge Prof. S. K. Arora for kindly providing the structural data for cyclized rifamycin SV and monoclinic rifamycin S and Prof. S. Cerrini for kindly providing the structural data for 4-deoxy-3′-bromopyrido[1′,2′,1,2]imidazo[5,4-c]rifamycin S. Thanks are also due to Dr. P. Ferrari for his valuable contribution and to Prof. G. Sferlazzo for discussion of the statistical results.

References

1. Haleblian, J. K., and W. McCrone. Pharmaceutical application of polymorphism. *J. Pharm. Sci.* **58**:911–929 (1969).
2. Haleblian, J. K. Characterization of habits and crystalline modification of solids and their pharmaceutical applications. *J. Pharm. Sci.* **64**:1269–1288 (1975).
3. Byrn, S. R. *Solid State Chemistry of Drugs*, Vol. 4. Academic Press, New York, 79–148 (1982).
4. Florence, A. T., and D. Attwood. *Physicochemical Principles of Pharmacy*, Ed. 2, Vol. 2. MacMillan, Houndmills, 21–46 (1988).
5. Cavalleri, B., M. Turconi, G. Tamborini, E. Occelli, G. Cietto, R. Pallanza, R. Scotti, M. Berti, G. Romanò, and F. Parenti. Synthesis and biological activity of some derivatives of rifamycin P. *J. Med. Chem.* **33**:1470–1476 (1990).
6. Wherli, W., and M. Staehelin. The rifamycins: relation of chemical structure and action on RNA polymerase. *Biochim. Biophys. Acta* **182**:24–29 (1969).
7. Sensi, P. Inhibitors of the transcribing enzymes. *Pure Appl. Chem.* **35**:383–410 (1973).
8. Brufani, M., S. Cerrini, W. Fedeli, and A. Vaciago. Rifamycins: an insight into biological activity based on structural investigations. *J. Mol. Biol.* **87**:409–435 (1974).
9. Lancini, G., and W. Zanichelli. Structure-activity relationships in rifamycin, in *Structure-Activity Relationship Among the Semisynthetic Antibiotics* (D. Perlman, ed.). Academic Press, New York, 531–600 (1977).
10. Brufani, M., L. Cellai, S. Cerrini, W. Fedeli, A. Segre, and A. Vaciago. Structure-activity relationships in the Ansamycins: Molecular structure and activity of 3-carbomethoxy-rifamycin S. *Mol. Pharmacol.* **21**:394–399 (1982).
11. Arora, S. K., and P. Main. Correlation of structure and activity in ansamycins: molecular structure of cyclized rifamycin SV. *J. Antibiot. (Tokyo)* **37**:178–181 (1984).
12. Pelizza, G., M. Nebuloni, P. Ferrari, and G. G. Gallo. Polymorphism of rifampicin. *Farm. Ed. Sci.* **32**:471–481 (1977).
13. Run-Zhong, L., and R. Fang. Studies on the characteristics of four types of crystalline rifandine. *Chin. J. Antibiot.* **12**:1–10 (1987).
14. Run-Zhong, L., and R. Fang. Crystal modification of rifandin. *Kangshengsu* **14**:301–306 (1989).
15. Arora, S. K. Correlation of structure and activity in ansamycins: structure, conformation and interactions of antibiotic rifamycin S. *J. Med. Chem.* **28**:1099–1102 (1985).
16. Arora, S. K., and P. Arjunan. Molecular structure and conformation of rifamycin S, a potential inhibitor of DNA-dependent RNA polymerase. *J. Antibiot. (Tokyo)* **45**:428–431 (1992).
17. Lehmann, M. S., and F. K. Larsen. A method for location of the peaks in step-scan-measured Bragg reflections. *Acta Crystallogr. Sect. A* **30**:580–584 (1974).
18. Burla, M. C., G. Cascarano, E. Fares, C. Giacovazzo, G. Polidori, and R. Spagna. From partial structure to complete structure. *Acta Crystallogr. Sect. A* **45**:781–786 (1989).
19. Sheldrick, G. M. SHELX76, a program for crystal structure determination. University of Cambridge, Cambridge, UK (1976).
20. Nardelli, M. PARST: a system of Fortran routines for calculating molecular structure parameters from results of crystal structure analyses. *Comput. Chem.* **7**:95–98 (1983).
21. Johnson, C. K. ORTEP: report ORNL-3794. Oak Ridge National Laboratory, Oak Ridge, TN (1965).
22. Motherwell, W. D. S., and W. Clegg. PLUTO: program for plotting molecular and crystal structures. University of Cambridge, Cambridge, UK (1976).
23. Stout, G. H., and L. H. Jensen. *X-Ray Structure Determination*. MacMillan, London, 303 (1972).
24. Taylor, R., O. Kennard, and W. Versichel. The geometry of the N-H· · ·C═O hydrogen bond. 3. Hydrogen-bond distances and angles. *Acta Crystallogr. Sect. B* **40**:280–288 (1984).
25. Cellai, L., S. Cerrini, A. Segre, M. Brufani, W. Fedeli, and A. Vaciago. A study on the structures of 3-methoxycarbonylrifamycins by X-ray crystallography and ^{1}H nuclear magnetic resonance spectroscopy. *J. Chem. Soc. Perkin Trans. II* 1633–1640 (1982).
26. Arora, S. K. Correlation of structure and activity in ansamycins: molecular structure of sodium rifamycin SV. *Mol. Pharmacol.* **23**:133–140 (1983).
27. Beeson, J. C., L. J. Fitzgerald, J. C. Gallucci, R. E. Gerkin, J. T. Rademacher, and A. W. Czarnik. π-Complexation in the solid state induced by intermolecular hydrogen bonding. *J. Am. Chem. Soc.* **116**:4621–4622 (1994).
28. Cerrini, S., D. Lamba, M. C. Burla, G. Polidori, and A. Nunzi. Structure of 21-acetoxy-11(*R*)-rifamycinol S: the role of the one- and two-phase semi-invariants in multisolution phasing methods. *Acta Crystallogr. Sect. C* **44**:489–495 (1988).
29. Cellai, L., S. Cerrini, D. Lamba, V. Brizzi, and M. Brufani. X-ray crystal structure and activity of rifamycinol, a semi-synthetic derivative of the antibacterial antibiotic rifamycin S showing a dimeric π-π complex in the crystal. *J. Chem. Res.* (suppl.) 328–329 (1987).
30. Bartolucci, C., L. Cellai, S. Cerrini, D. Lamba, A. L. Segre, V. Brizzi, and M. Brufani. Synthesis, reactivity studies, and X-ray crystal structure of (11*R*)-25-*O*-deacetyl-11-deoxo-11-hydroxy-21,23-*O*-isopropylidenerifamycin S. *Helv. Chim. Acta* **73**:185–198 (1990).
31. Leger, J. M., and A. Carpy. Structure cristalline d'une thiazolorifamycine: rifamycine P. *Helv. Chim. Acta* **74**:326–330 (1991).
32. Gadret, M., M. Goursolle, J. M. Leger, and J. C. Colleter. Structure cristalline de la rifampicine. *Acta Crystallogr. Sect. B* **31**:1454–1462 (1975).
33. Arora, S. K. Structural investigations of mode of action of drugs. III. Structure of rifamycin S iminomethyl ether. *Acta Crystallogr. Sect. B* **37**:152–157 (1981).
34. Brufani, M., L. Cellai, S. Cerrini, W. Fedeli, and A. Vaciago. Structure-activity relationships in the ansamycins: the crystal structure of tolypomycinone. *Mol. Pharmacol.* **14**:693–703 (1978).
35. Brufani, M., L. Cellai, S. Cerrini, W. Fedeli, E. Marchi, A. Segre, and A. Vaciago. X-ray crystal structure of 4-deoxy-3′-bromopyrido[1′,2′-1,2]imidazo[5,4-c]rifamycin S. *J. Antibiot. (Tokyo)* **37**:1623–1627 (1984).
36. Bartolucci, C., L. Cellai, S. Cerrini, P. Di Filippo, and D. Lamba. X-ray crystal structure of 25-*O*-deacetyl-27,28-didehydro-27-demethoxy-11-deoxo-11,29-epoxy-28,29-dihydro-21,23-*O*-isopropylidenerifamycin S. *Helv. Chim. Acta* **75**:153–159 (1992).
37. Allen, F. H., and O. Johnson. Automated conformational analysis from crystallographic data. 4. Statistical descriptors of a distribution of torsion angles. *Acta Crystallogr. Sect. B* **47**:62–67 (1991).

Send reprint requests to: Giancarlo Pelizzi, Universita Degli Studi Parma, Dipartimento di Chimica Generale ed Inorganica, Viale delle Scienze, I-43100 Parma, Italy.